Soft Matter

ARTICLE TYPE

Cite this: DOI: 00.0000/xxxxxxxxxx

Relative contributions of chain density and topology to the elasticity of two-dimensional polymer networks

Ghadeer Alamé,[a] and Laurence Brassart*[a]

Received Date
Accepted Date

DOI: 00.0000/xxxxxxxxxx

Understanding the relationships between the structure of polymer networks and their mechanical properties is important for the design of advanced soft materials with optimal properties. However, classical rubber elasticity theories often fall short in their description of the network structure, while simulation techniques at molecular scale remain impractical at that length scale. Here we develop a computational approach based on random discrete networks, in which the polymer network is represented as an assembly of non-linear springs connected at crosslinking points. The density of elastically-effective chains, average network coordination and chain contour lengths are varied independently in order to identify their respective contributions to the network elasticity. Numerical results suggest scaling relations between network parameters and elastic properties that are markedly different from the predictions of classical rubber elasticity theories. In particular, the elastic modulus of 2D random networks is found to be independent of density at constant topology, and proportional to the average coordination at constant density. The discrepancy is due to the pre-straining of the chains in the discrete network, which is not accounted for in classical models of rubber elasticity. Our results have implications for the interpretation of experimental data for ideal network gels that are formed by the cross-coupling of macromolecular building blocks in solution

1 Introduction

Many soft materials, such as elastomers and hydrogels, are made of long chain molecules crosslinked to form a three-dimensional network. Their mechanical properties depend on the entropy-dominated elastic response of the individual chains and on the network topology, which dictates the partitioning of stretch among the chains. Key topological parameters include the chain density, chain length distribution and the crosslink coordination.[1] Topological defects (dangling chains, loops), spatial heterogeneities and trapped entanglements are also known to impact the mechanical behaviour of polymer networks.[2–5] Understanding the relationships between the structure of polymer networks and their mechanical properties is important for the design of advanced soft materials with optimal properties.

In recent years, a new paradigm for gel formation has been introduced, whereby ideal covalent networks are produced by the cross-coupling of macromolecular building blocks.[6–10] Notably, "ideal network" gels were produced by the cross-coupling of 4-arm PEG macromolecules with well-defined chain length[11] (Fig. 1). These model gels were shown to possess a very high compressive strength, close to cartilage,[3] which was attributed to the highly homogeneous network structure, essentially free of entanglements and with few topological defects.[12,13] Ideal networks constitute an excellent model system to investigate structure-property relationships in hydrogels,[4,14–17] as well as a promising platform for the design of new materials with tuneable properties.[18–20] The modelling strategy adopted in the present work is directly motivated by these ideal network gels.

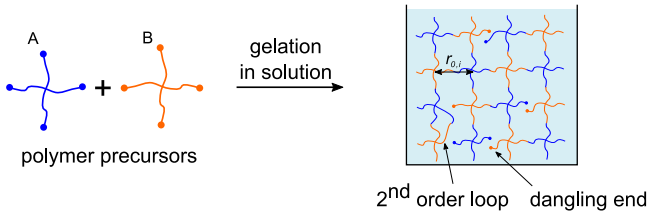

Fig. 1 Ideal polymer networks are formed by the mutual reaction of macromolecular building blocks in solution, typically four-arm macromonomers with identical arm length. The building blocks have end-linking groups of type "A" or "B" that are mutually reactive, while avoiding self-reaction. Ideal networks are essentially free of entanglements and possess few defects such as dangling ends and loops.

The elasticity of polymer networks is usually described within

[a] *Department of Materials Science and Engineering, Monash University, Clayton, VIC 3800, Australia. E-mail: laurence.brassart@monash.edu*

the framework of rubber elasticity theory,[1,21] in which the network is represented as an assembly of freely-jointed chains behaving like entropic springs. For example, the classical Affine[21–23] and Phantom[24,25] models have been widely used to correlate the elastic modulus to the chain density and average coordination of the network. These models assume that the distribution of the end-to-end distances of the network strands obey the Gaussian statistics of a freely-jointed chain. Large-deformation theories based on non-Gaussian chain statistics are usually formulated by considering a unit cell of representative chains sampling the orientation space and with force-extension relationship described by Langevin statistics. Well-known models include the non-Gaussian 3-chain,[26] 4-chain,[27] 8-chain[28] and full-network[29] models, see also the review by Boyce and Arruda.[30] A major limitation of all these models is that they fall short in describing the effect of network topology on the mechanical properties.

Computational Discrete Network (DN) models constitute an interesting alternative approach to investigate structure-property relationships in polymer networks. Like in rubber elasticity theories, chains are represented as entropic springs with force-extension relationship corresponding to a freely-jointed chain, while the partitioning of stretch among the chains is dictated by the condition of mechanical equilibrium. DN models can consider a large number of randomly oriented chains, thus enabling the explicit representation of a number of topological features, such as chain length distribution, coordination of the crosslinking points, or topological defects such as dangling ends and loops. Their computational cost is also much lower than that of molecular dynamics simulations.

DN models have been used previously to investigate structure-property relationships in polymer networks. Early studies used regular lattices of linear, mainly Hookean springs to investigate critical phenomena (i.e. connectivity and rigidity percolation) in relation to gelation of polymer networks.[31–35] More recently, DN models have been developed to investigate various features of the large deformation behaviour of flexible polymer networks, including extensibility limit, damage or unfolding of secondary structures.[36–39] Similar computational models have been extensively developed for semi-flexible chains and filaments, which possess bending stiffness.[40,41] Another area where DN models were proved successful is for the modelling of biological 2D networks, which are found in various cellular structures as reinforcement of plasma or nuclear membranes. Such networks may be classified according to their connectivity, with the 3-fold, 4-fold and 6-fold types of connectivity being the most-commonly encountered.[42] A widely-studied example of biological 2D network is the membrane-associated cytoskeleton of the Red Blood Cell (RBC), which can be represented as a nearly-perfect triangular network. DN-based studies of the RBC mechanics include the investigation of topology-property relationships in the plane as well as simulations of curved surfaces.[43–47] In the context of ideal synthetic networks such as tetra-arm PEG hydrogels considered here, only a few studies based on DN models have been reported, which include some comparison with experimental data.[38,48] However, to the best of our knowledge, a systematic study of structure-property relationships in such networks has not been presented yet.

In this work, we develop a computational framework based on discrete networks to systematically investigate the relative contributions of chain density, average crosslink coordination and chain contour length on the elasticity of random networks. This study is limited to two dimensions for simplicity, but generalisation to three dimensions is conceptually similar. Inspired by ideal network gels, we focus on monodispersed system, i.e. we assume that all the polymer strands between two crosslink points have the same contour length. We also assume that the network is free of entanglements and loops, but we account for the presence of dangling ends by varying the coordination of crosslinking points. By considering 2D, possibly-defected networks of 3-fold, 4-fold and 6-fold coordination, this study is also relevant to biological, membrane-associated networks. Computational results are compared to analytical predictions provided by analytical models in 2D, including non-Gaussian 2-chain, 4-chain and full-network models. We also compare our results in the small deformation regime to the classical Affine and Phantom models.

DN simulation results provide scaling relations between the elastic modulus and network parameters that contradict the predictions of classical rubber elasticity theories. The elastic modulus of 2D networks is found to be independent of the chain density at constant topology, but scales linearly with the average coordination at constant density. The modulus is also found to be inversely proportional to the number of Kuhn segments in the strands. These results are explained by the coupling between chain prestraining and network parameters in the DN model, which is not taken into account in rubber elasticity theories. Analytical and computational predictions are reconciled when the dependency of the initial chain end-to-end distance on density and average coordination is taken into account in analytical models. Our results have implications for the interpretation of experimental data for ideal network gels.

2 Modelling of 2D Random Networks

2.1 Discrete network generation

We consider periodic random networks consisting of n identical chains in a square domain of size L in the undeformed configuration. The density of chains (number of chains per unit area) is given by:

$$\nu = \frac{n}{L^2}. \tag{1}$$

The number of chains is chosen sufficiently large to ensure that the network is statistically representative. For a random network with n chains and density ν, the length L is set by relation (1). We describe the topology of random network in terms of the average crosslink coordination $\bar{\phi}$, i.e., the average number of chains meeting at each crosslinking point.

Random network geometries were produced starting from unstructured finite element meshes generated with the open-source meshing software GMSH.[49] First, seeds were randomly distributed in the simulation domain prior to meshing to enforce mesh randomness and ensure isotropic mechanical behaviour. Perfectly-coordinated networks with crosslink coordination $\bar{\phi} = 3$ were obtained starting from triangle meshes by placing crosslink-

ing points at the element centres and connecting them through the triangle edges. The coordination of each interior crosslinking point is then exactly 3. Networks with $\bar{\phi} = 4$ were obtained using a similar procedure but starting from quadrangle meshes. Networks with $\bar{\phi} = 6$ were generated starting from triangle meshes by identifying the triangle vertices with crosslinking points. In that case the coordination of crosslinks is not uniform but fluctuates about an average value of about 6. Examples of random networks with $\bar{\phi} = 3$, 4 and 6 are shown in Figs 2(a)-(c).

Networks with intermediate average coordination values $\bar{\phi} \in [2,6]$ were obtained starting from perfectly-coordinated networks with $\bar{\phi} = 3$, 4 or 6 and by randomly removing chains with a certain probability $(1-p)$ (i.e. $p = 1$ corresponds to the "perfect", as-generated network), as represented in Figs 2(d)-(f). In the following we use the notation $Z = 3$, 4 or 6 to refer to the coordination of the original network before removing chains. Since this procedure causes some of the remaining chains to become elastically ineffective (i.e. they do not transmit any force when the network is under load), those elastically-ineffective chains were systematically removed from the network. In the following, the number of chains n is always taken as the number of elastically-effective chains. Likewise, the density ν always represents the density of elastically-effective chains, according to Eq. (1).

2.2 Single chain behaviour

We represent polymer strands between crosslinking points as Freely-Jointed Chains (FJC) consisting of N Kuhn segments with length b, with N and b identical in all strands. Consistent with a 2D representation, we assume that the chain conformations are confined to a planar surface. This situation is representative of polymers physically adsorbed on a surface or polymers confined to an interface between two phases. In 3D, the force-extension relationship of a FJC is described by the Langevin function $\mathscr{L}(x) = \coth(x) - 1/x$.[50] This relationship is obtained from statistical mechanics considerations for constant force and temperature. A similar approach in 2D leads to the following force-extension relationship:[51]

$$\frac{r}{Nb} = \frac{I_1(\beta)}{I_0(\beta)} \equiv \mathscr{L}_{2\mathrm{D}}(\beta), \tag{2}$$

where r is the average chain end-to-end distance and β is the normalised force: $\beta = \frac{fb}{kT}$, with f the applied force, k the Boltzmann constant and T the absolute temperature. The function $I_\nu(\beta)$ is the modified Bessel function of the first kind of order ν. The function $\mathscr{L}_{2\mathrm{D}}$ plays the same role as the Langevin function in the 3D FJC model. The corresponding Helmholtz free energy of a chain is:

$$w(r) = kTN\left(\frac{r}{Nb}\beta - \log(I_0(\beta))\right), \tag{3}$$

where β is related to r by the force-extension relation (2).

For small elongation ($r \ll bN$), relation (2) is approximately linear:

$$\frac{r}{Nb} = \frac{\beta}{2} \quad \text{for} \quad \beta \ll 1. \tag{4}$$

(In the 3D FJC model, the denominator in the right-hand side is 3.) In practice, the linear approximation is accurate as long as $r/Nb \leq 0.3$. The force tends to infinity when r approaches the contour length Nb. The force-extension relationship is qualitatively similar to that of the 3D FJC, and therefore we can assume that our results would remain qualitatively the same if the 3D FJC model was used instead.

2.3 Network behaviour

Random networks of given density and average crosslink coordination were subjected to prescribed macroscopic stretches $\lambda_1 = l_1/L$ and $\lambda_2 = l_2/L$, where l_1 and l_2 are the lengths of the simulation domain in directions 1 and 2 in the deformed configuration. We assume incompressibility: $\lambda_1\lambda_2 = 1$ and applied tension in direction 1 ($\lambda_1 \geq 1$). For given values of the macroscopic stretches, the positions of the interior crosslink points were calculated from the conditions of mechanical equilibrium. In practice, these positions were found by minimising the elastic energy of the network:

$$W = \frac{1}{L^2}\sum_{i=1}^{n} w^{(i)}, \tag{5}$$

where the chain energy function w is given by Eq. (3) and depends on the end-to-end distance of the chain. The chain end-to-end distribution thus depends on the applied macroscopic stretches, as well as on the network density and topology. Energy minimisation was also carried out in the undeformed state $\lambda_1 = \lambda_2 = 1$, since the network generation procedure outlined in Section 2.1 does not produce self-equilibrated networks. Networks shown in Fig. 2 are equilibrated configurations obtained after this initial relaxation step in the undeformed state.

Numerical simulations were carried out using the open-source molecular dynamics software LAMMPS,[52] treating the crosslinking points as atoms and the polymer chains as bonds with user-defined behaviour corresponding to the force-extension relationship (2). Since Eq. (2) cannot be solved analytically for the force, a polynomial approximation of the Bessel functions was used.[53] Principal nominal stresses P_1 and P_2 (force per unit of undeformed length) were calculated from the reaction forces on the boundary nodes, and the corresponding Cauchy stresses were calculated from the relations $\sigma_1 = P_1/\lambda_2$ and $\sigma_2 = P_2/\lambda_1$.

In the DN model, vanishing macroscopic stresses correspond to the collapsed state of the network. This follows from the force-extension relationship (2), in which a zero force corresponds to a vanishing mean chain end-to-end distance. Consequently, a tensile hydrostatic stress is needed to maintain a finite volume. In real networks, network collapse is prevented by physical effects such as excluded volume or the presence of a solvent (osmotic pressure). These effects are not explicitly accounted for in the present model. However, due to incompressibility the macroscopic response is independent of the hydrostatic stress, and therefore here we only consider the stress difference $(\sigma_1 - \sigma_2)$. The elastic modulus of the 2D network is defined as the initial slope of the macroscopic stress-stretch relation:

$$E = \lim_{\lambda_1 \to 1} \frac{d(\sigma_1 - \sigma_2)}{d\lambda_1}, \tag{6}$$

where the principal stress difference is taken as a function of λ_1

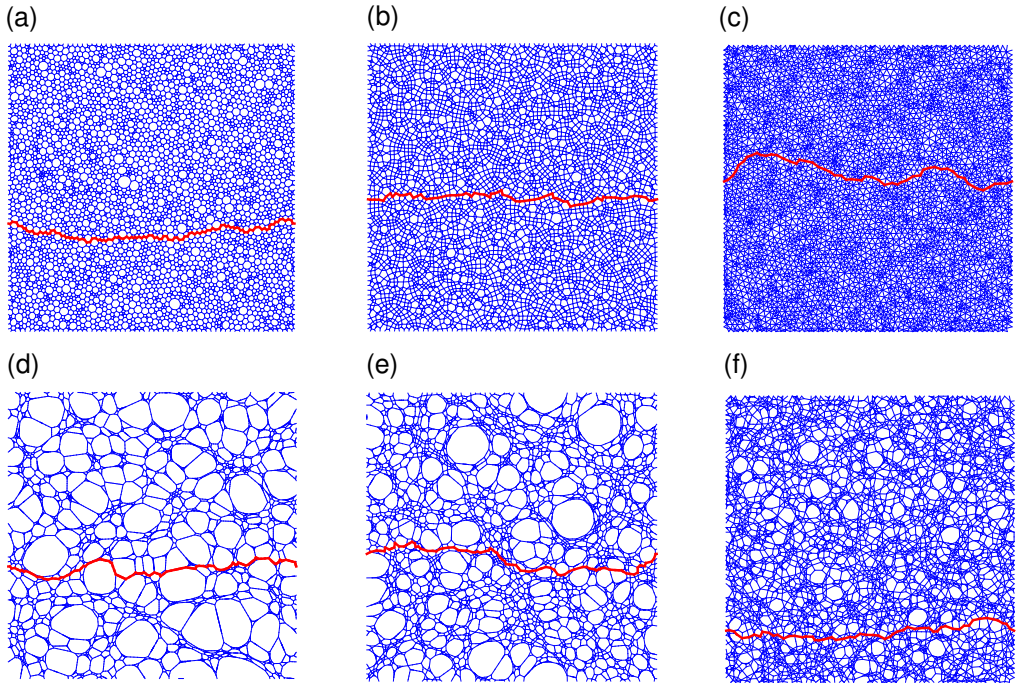

Fig. 2 (a)-(c) Random networks with coordination $\bar{\phi} = 3$, 4 and 6 ($Z = 3$, 4 and 6) having about 12500 chains. (d)-(f) Random networks obtained by removing chains from random networks with respectively $Z = 3$, 4 and 6 and $p = 0.8$. The number of chains are about 9500 and the resulting average coordination values are (d) $\bar{\phi} = 2.49$, (e) $\bar{\phi} = 3.21$ and (f) $\bar{\phi} = 4.79$. All networks are represented in their equilibrium configuration in the undeformed state $\lambda_1 = \lambda_2 = 1$. The shortest chain path along the tensile loading direction is indicated in red in each network.

only (since $\lambda_2 = 1/\lambda_1$). Under the assumption of incompressibility, we can always superimpose on the calculated state of stress a mean stress such that $\sigma_2 = 0$, with no effect of the stretches. The above modulus is thus identified with the Young modulus of the incompressible 2D network.

The maximum extensibility of the network is defined as the stretch λ_1 at which the macroscopic stress asymptotically tends to infinity. This value is difficult to calculate accurately due to convergence problems arising at large stretches in the computational model. As an alternative measure, we consider the shortest chain path between the left and right boundaries of the domain, and estimated the maximum stretch by the sum of the contour lengths of all the chains belonging to this path, divided by the initial length of the domain:

$$\lambda_{max} = \frac{n_s N b}{L}, \tag{7}$$

with n_s the number of chains in the shortest path. The advantage of this measure is that it only depends on the network topology and does not require a mechanical analysis. The shortest path of random network was identified using Dijkstra's algorithm[54] available in the NetworkX package of Python. The shortest chain path is represented in red on the networks in Fig. 2. Eq. (7) indicates that the maximum extensibility scales linearly with the number of Kuhn segments. Since the length L is set by relation (1), it also means that the maximum extensibility scales with $\nu^{1/2}$, whereas the network topology at fixed density impacts the maximum extensibility via n_s in an implicit manner.

3 Analytical models

DN models can provide detailed predictions for random network with almost arbitrary topology. Yet, the computational cost is relatively high, and analytical constitutive theories remain essential for large scale simulations of soft structures. Here we consider three 2D models, which are the counterparts of well-known models of rubber elasticity in 3D, namely the 3-chain model,[26] 8-chain model[28] and full-network model.[29] These models consider a set of representative chains sampling the orientation space in the undeformed configuration of the network and which deform affinely with the macroscopic stretches. Like in the DN model, the force-extension relationship of individual chains is described by the 2D FJC model, Eq. (2). DN simulations and analytical models differ in their representation of the network architecture and modelling of the partitioning of stretches among the chains. One of the objectives of this study is to assess the predictive capability of these three models, using the DN results as reference results.

2-chain model: The 2-chain model considers two representative chains with identical initial end-to-end distance r_0 aligned with the principal stretch directions. In the deformed configuration, the chain end-to-end distances become

$$r^{(1)} = \lambda_1 r_0, \quad r^{(2)} = \lambda_2 r_0, \tag{8}$$

where the superscript i refers to chain i in the unit cell. Using Eqs (3) and (5), the free energy per unit volume of the network is

obtained:

$$W = \frac{kTN\nu}{2}\left[\frac{\lambda_1 r_0}{Nb}\beta^{(1)} + \log I_0(\beta^{(1)}) + \frac{\lambda_2 r_0}{Nb}\beta^{(2)} + \log I_0(\beta^{(2)})\right], \tag{9}$$

where we gave a density $\nu/2$ to each representative chain. The stress-stretch relations is calculated as:

$$\sigma_1 - \sigma_2 = \lambda_1 \frac{\partial W}{\partial \lambda_1}\Big|_{\lambda_2} - \lambda_2 \frac{\partial W}{\partial \lambda_2}\Big|_{\lambda_1}, \tag{10}$$

giving:

$$\sigma_1 - \sigma_2 = \frac{1}{2}(kTN\nu)\left(\frac{r_0}{Nb}\right)\left(\beta^{(1)}\lambda_1 - \beta^{(2)}\lambda_2\right). \tag{11}$$

The maximum extensibility of the network is reached when the chain aligned with the first principal direction reaches the contour length, $r^{(1)} = Nb$, giving:

$$\lambda_{max} = \frac{Nb}{r_0}. \tag{12}$$

4-chain model: The 4-chain model considers a square unit cell with four chains connecting each vertex to the centre of the cell. The unit cell deforms with the macroscopic principal stretches. It follows that all chains have the same end-to-end distance, $r = \Lambda r_0$, where the chain stretch Λ is given by:

$$\Lambda = \frac{\sqrt{\lambda_1^2 + \frac{1}{\lambda_1^2}}}{\sqrt{2}}. \tag{13}$$

The free energy per unit volume of the network is:

$$W = kTN\nu\left(\frac{r_0\Lambda}{Nb}\beta + \log I_0(\beta)\right), \tag{14}$$

and the stress-stretch relation is given by:

$$\sigma_1 - \sigma_2 = \frac{1}{2}kTN\nu\left(\frac{r_0}{Nb}\right)\frac{\beta}{\Lambda}(\lambda_1^2 - \frac{1}{\lambda_1^2}). \tag{15}$$

The maximum extensibility corresponds to $\Lambda = Nb/r_0$:

$$\frac{\sqrt{\lambda_{max}^2 + \frac{1}{\lambda_{max}^2}}}{\sqrt{2}} = \frac{Nb}{r_0}. \tag{16}$$

Full-network model: The full-network model considers a distribution of identical chains with initial end-to-end distance r_0 and random orientation. Each chain is assumed to deform affinely with the macroscopic stretches. The stretch of a given chain, $\Lambda(\theta) = r(\theta)/r_0$ then depends on its orientation in the undeformed configuration, described by the angle θ between the chain end-to-end vector and the first principal axis. The chain stretch as a function of θ is given by:

$$\Lambda(\theta) = \sqrt{\cos^2\theta\lambda_1^2 + \sin^2\theta\lambda_2^2}. \tag{17}$$

The free energy density of the network is obtained by volume averaging of the individual chain energies over all the orientations:

$$W = \frac{\nu}{2\pi}\int_0^{2\pi} kTN\left(\frac{r_0}{Nb}\Lambda(\theta)\beta(\theta) - \log(I_0(\beta(\theta)))\right)d\theta. \tag{18}$$

Using Eq. (10), the stress-stretch relation is obtained:

$$\sigma_1 - \sigma_2 = kTN\nu\left(\frac{r_0}{Nb}\right)\frac{1}{2\pi}\int_0^{2\pi}\frac{\lambda_1^2\cos^2\theta - \lambda_2^2\sin^2\theta}{\Lambda}\beta(\theta)d\theta. \tag{19}$$

The maximum stretch is found when chains aligned with the first principal direction (i.e. with $\theta = 0$ and $\Lambda = \lambda_1$) reach their contour length, so that the maximum extensibility is simply expressed as:

$$\lambda_{max} = \frac{Nb}{r_0}. \tag{20}$$

This is the same extensibility as the extensibility predicted by the 2-chain model.

In the Gaussian limit of small chain stretch ($\frac{r_i}{Nb} \leq 0.3$), all three models give the same stress-stretch relation:

$$\sigma_1 - \sigma_2 = (kTN\nu)\left(\frac{r_0}{Nb}\right)^2\left(\lambda_1^2 - \frac{1}{\lambda_1^2}\right), \tag{21}$$

and the modulus defined by Eq. (6) is given by:

$$E^{\text{Gauss}} = 4(kTN\nu)\left(\frac{r_0}{Nb}\right)^2. \tag{22}$$

Rubber elasticity models usually assume that the parameter r_0 is independent of density. For example, for a dry network r_0 is often identified with the root-mean-square (rms) value of the end-to-end distance of a freely-jointed chain under no force, $r_0 = \sqrt{N}b$, regardless of the chain density in the network. It then follows from Eq. (22) that the modulus is proportional to density and independent of N.

In contrast, in DN models the distribution of chain end-to-end distances cannot be prescribed a priori, as it intrinsically depends on density and network topology. As shown in the next section, the dependence of r_0 on density leads to the loss of proportionality between elastic modulus and density at fixed topology. In the next section, we identify the relationship between r_0, density and network topology parameters to be used in Eq. (22) from DN simulations.

4 Results

4.1 Evolution of initial chain end-to-end distance with network parameters

In a discrete network model of given density and topology, the distribution of the chain end-to-end distances is dictated by the condition of mechanical equilibrium under prescribed macroscopic stretches. We define the initial rms average chain end-to-end distance as:

$$\bar{r}_0 = \left(\frac{1}{n}\sum_{i=1}^{n}\left(r_0^{(i)}\right)^2\right)^{1/2}, \tag{23}$$

where $r_0^{(i)}$ is the initial end-to-end distance of the i^{th} chain in the equilibrated, undeformed configuration of the network ($\lambda_1 = \lambda_2 = 1$). The rms average is used in reference to the classical description in rubber elasticity theory. In our simulations, the number of chains n in a network of given topology is kept constant, and the simulation length is calculated from the desired density as $L = (n/\nu)^{\frac{1}{2}}$, according to Eq. (1). It follows that the initial chain

end-to-end distances also scale with $\nu^{-\frac{1}{2}}$, that is, increasing density at constant topology requires "compressing" the chains. The relationship between average chain pre-stretch and density is illustrated in Fig. 3(a) for random networks with $\bar{\phi} = 3$, 4 and 6. The scaling of the initial average chain end-to-end distance with density is clear from the inset in the figure.

At constant density, the initial average chain end-to-end distance also depends on the average coordination of the crosslinking points, as illustrated in Fig. 3(b). As seen in the inset of this figure, the initial average end-to-end distance scales with the square root of the average coordination, and tends to zero when the average coordination tends to a critical minimal value near the percolation threshold. When approaching the percolation limit, only a few paths of highly extended chains span the simulation domain, while the majority of chains have almost collapsed ($r_0^{(i)} \approx 0$), so that on average $\bar{r}_0$ is close to zero. The inset in Fig. 3(b) also suggests that $\bar{r}_0$ depends on Z, for a given value of $\bar{\phi}$. This indicates that network topology is not completely described by average network coordination alone, and that other topological factors (which depend on the network generation procedure) also govern the initial chain end-to-end distance distribution. In the rest of this study, we neglect the effect of the Z-value of the initial, perfectly-coordinated network and identify the scaling relation by performing a single regression for the three curves represented in Fig. 3(b).

Based on the numerical results of Figs 3(a) and 3(b), we propose that $\bar{r}_0^2$ scales with density and average coordination as $\frac{\alpha\bar{\phi}+\beta}{\nu}$, where α and β are regression parameters assumed identical for all Z values (note that the scaling with ν is "exact" since it directly follows from geometry). The best-fit scaling relation over all three Z-values is remarkably simple:

$$\bar{r}_0^2 = \frac{\bar{\phi} - \bar{\phi}_c}{\nu}, \tag{24}$$

where $\bar{\phi}_c = 2$ represents the average coordination at the percolation threshold. The prediction of Eq. (24) is represented by the continuous black lines in Figs 3(a) and 3(b). The discrepancy between numerical and analytical predictions in Fig. 3(a) is due to the regression error in Fig. 3(b) for the corresponding value of average coordination.

It is worth noting that $\bar{r}_0$ is independent of the number N of Kuhn segments. While N impacts the force necessary to maintain a chain end-to-end distance, it does not impact the equilibrium positions of the crosslinking points in the network. As shown in the following, the dependence of initial chain end-to-end distance on network parameters is key to understand the relationships between network parameters and mechanical properties. Likewise, analytical model predictions agree with DN simulations only when the dependence of r_0 on density and average coordination is taken into account.

4.2 Effect of network parameters on mechanical properties

Figs 4(a) and 4(b) show the evolution of modulus with density and average network coordination, as predicted by the DN model. The modulus is mainly independent of density, except at very low

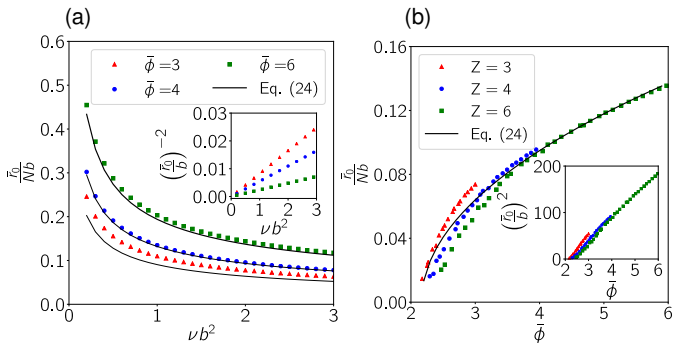

Fig. 3 Normalised rms average of the initial chain end-to-end distance as a function of (a) normalised density ($\bar{\phi} = Z = 3$, 4 and 6) and (b) the network average coordination for $\nu b^2 = 0.02$. In both figures the number of Kuhn segments is $N = 100$. Different symbols refer to the perfectly-coordinated network (with coordination $Z = 3$, 4 and 6) from which the actual network with intermediate coordination was obtained by randomly cutting chains in (b). The continuous black lines correspond to relation (24).

density values, where it tends to infinity as density approaches zero. These trends directly follow from the dependence of the initial chain length distribution on density. Indeed, increasing density at constant coordination leads to a decrease in the initial chain end-to-end distances (Fig. 3(a)), which in turn reduces the energy stored in the chains in the initial configuration. At moderate to high density values, the energy reduction brought about by a decrease in the initial chain length exactly compensates the increase in free energy due to an increase in density, and the modulus is independent of density. A low density values however, chains are initially pre-stretched beyond their Gaussian limit ($\frac{r_0}{Nb} > 0.3$). When density further decreases, the increase in elastic energy stored in the highly pre-stretched chains dominates, and the modulus increases. These trends are well reproduced by the analytical estimate of the modulus (22), with r_0^2 given by Eq. (24).

In contrast, the modulus depends markedly on average coordination for a constant density (Fig. 4(b)). The figure shows numerical results for networks with average coordination ranging from $\bar{\phi} \approx 2$ (near the percolation threshold) to $\bar{\phi} = 6$, which were obtained by randomly removing chains from perfectly-coordinated networks with $Z = 3$, 4 or 6. Density was kept constant by scaling the domain dimensions using relation (1). The value of density used here ($\nu b^2 = 0.02$) ensures that chains are in their Gaussian regime in the undeformed configuration, cf. Fig. 3(a). Predictions of Eq. (22) are also shown, in which r_0^2 was calculated from Eq. (24). The good agreement indicates that the modulus scales as $(\bar{\phi} - \bar{\phi}_c)$, with vanishing modulus at $\bar{\phi}_c$. For given density and average coordination, the modulus also depends on the coordination Z of the original random network before the chain removal procedure. The modulus is lower in networks with a large Z value, i.e. networks from which more chains had to be removed to reach the desired average coordination $\bar{\phi}$. As previously mentioned, this indicates that average coordination does not fully characterise the topology of random networks, and that other factors impact the mechanical behaviour. However, the

variation in modulus between networks with different Z values can be seen as a second-order effect compared to the clear linear dependence of modulus on average coordination.

Figs 4(c) and 4(d) show the effect of density and average coordination on the maximum extensibility of random networks estimated based on the shortest path distance using Eq. (7). Predictions of the 2-chain model (or equivalently the full-network model), Eqs (12) and (20) are also shown, in which r_0^2 was estimated by relation (24). The maximum extensibility scales with the square root of density (Fig. 4(c)), which immediately follows from definition (7) of the maximum stretch and accounting for relation (1) between the domain size and density. Physically, since chains have lower initial end-to-end distance at high density (Fig. 3(a)), they can accommodate a larger stretch before reaching their contour length. The same scaling is predicted by the analytical models with r_0 estimated by (24). On the other hand, the maximum extensibility scales with $\bar{\phi}^{-\frac{1}{2}}$ (Fig. 4(d)), with infinite extensibility at the percolation limit. This can be understood based on the evolution of the chain initial end-to-end distance with coordination (Fig. 3(b)). At constant density, chains in networks with low coordination have a lower degree of initial pre-stretch than chains in networks of higher coordination, and can thus accommodate a larger applied stretch before reaching their contour length.

Finally, Fig. 5 shows the evolution of elastic modulus and maximum extensibility of the network as a function of the number of Kuhn segments N in the chains. The modulus scales with N^{-1} (Fig. 5(a)), in good agreement with the model (22) with r_0^2 calculated from Eq. (24). In other words, networks are softer when the number of Kuhn segments in the chains increases. On the other hand, the maximum extensibility scales linearly with N (Fig. 5(b)), in agreement with the analytical prediction (12), again estimating r_0^2 by (24).

4.3 Comparison between analytical models and discrete network predictions

We next compare the stress-stretch curves predicted by the analytical models to reference DN simulations for $\bar{\phi} = 3$ and 4, with $\nu b^2 = 0.02$ and $N = 100$. In the analytical models, r_0 was calculated from Eq. (24), giving $\bar{r}_0/Nb = 0.07$ for $\bar{\phi} = 3$ and $\bar{r}_0/Nb = 0.1$ for $\bar{\phi} = 4$. Network topology is thus accounted for in a implicit manner in the analytical models via the value of r_0.

The comparison is shown on Fig. 6. Results show the expected nonlinear relationship between stress and stretch, with the stress first increasing linearly at low stretches, before showing strongly non-linear behaviour once the chains enter their non-Gaussian regime. The macroscopic stress then tends to an infinite value as the macroscopic stretch approaches the maximum extensibility of the network. All three analytical models predict virtually the same behaviour at small to moderate stretches (all three models predict the same modulus (22) in the Gaussian regime), in good agreement with DN simulations. However, models differ at large stretches. The 4-chain model is found to significantly underestimate the stress for both coordination values. In the case $\bar{\phi} = 3$, the full-network model is in good agreement with the discrete network results at all stretches, while the 2-chain model is more accurate in the case $\bar{\phi} = 4$. The 2-chain and full-network models both include representative chains aligned with the tensile loading direction, leading to a stiffer response than the 4-chain model. This suggests that the discrete network behaviour is dominated by those chains that are initially aligned with the principal loading direction.

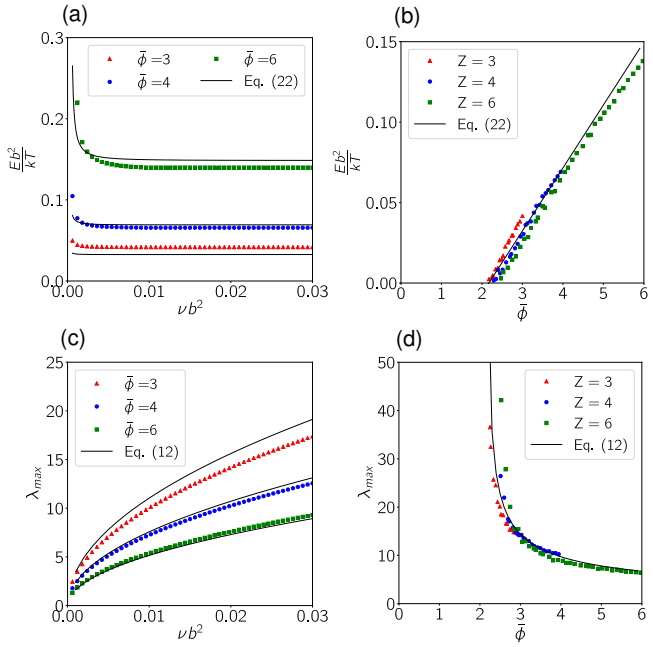

Fig. 4 Evolution of the normalised elastic modulus with (a) density ν and (b) average coordination of the network with $\nu b^2 = 0.02$; evolution of the maximum extensibility with (c) density and (d) average coordination of the network with $\nu b^2 = 0.02$. The number of Kuhn segments is $N = 100$ in all simulations. In (a) and (c), networks with $Z = \bar{\phi} = 3.\ 4$ and 6 were considered, and density was varied by scaling the simulation domain according to Eq. (1). In (b) and (d), networks of varying coordination were produced by randomly removing chains from initially perfectly-coordinated networks with $Z = 3,\ 4$ or 6, while density was kept at a constant value by scaling. Continuous black lines in (a) and (b) show the estimate of the modulus (22), and continuous black lines in (c) and (d) the estimate of the extensibility (12). In the analytical models, r_0^2 was estimated by relation (24).

5 Discussion

We have used discrete network simulations to identify the relative contributions of chain density, average network coordination and number of Kuhn segments per chain on the mechanical properties of 2D random networks. The elastic modulus was found to scale as $E \sim \frac{\bar{\phi}}{N}$, and to be independent of the density of elastically-effective chains. These trends are well reproduced by the analytical estimate (22), provided that the dependence of the initial end-to-end distance r_0 on density and average coordination is taken into account.

These results are explained from mechanical considerations. When density increases at constant topology, the average initial chain length decreases (Fig. 3(a)), which reduces the elastic energy stored in the chains. This energy decrease exactly balances

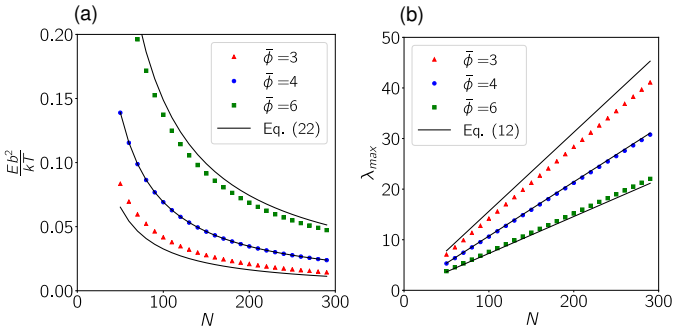

Fig. 5 Evolution of (a) elastic modulus and (b) maximum extensibility with the number of Kuhn segments N in the chains at constant density and average functionality, for $\nu b^2 = 0.02$. Continuous black lines correspond (a) Eq. (22) and (b) Eq. (12), in which r_0^2 was estimated by relation (24).

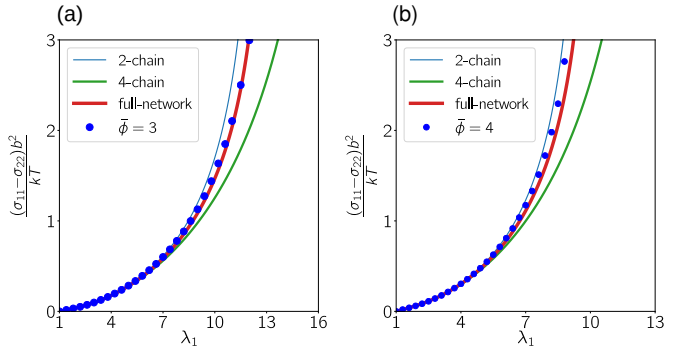

Fig. 6 Stress-stretch response of networks with (a) $\bar{\phi} = 3$ and (b) $\bar{\phi} = 4$, for $N = 100$ and $\nu b^2 = 0.02$. In the analytical model, r_0 was calculated from Eq. (24).

the increase in energy due to adding more chains per unit area in the network, and as a result the modulus remains constant. When average coordination increases at constant density, the average initial chain length increases, and the modulus also increases. The decrease of modulus with N follows from the fact that individual chains are more flexible when N increases, cf. Eq. (4).

Our results contradict the predictions of widely-used rubber elasticity models such as the Affine and Phantom models, which both assume that the initial end-to-end length distribution is independent of density and topology. In 2D, the Affine model gives $E^{\text{Affine}} = 4kT\nu$ (see Appendix), which coincides with expression (22) when $r_0 = \sqrt{N}b$. The Phantom model predicts a lower value of the modulus compared to the Affine model by accounting for the fluctuations of the crosslinks: $E^{\text{Phantom}} = E^{\text{Affine}}\left(1 - \frac{2}{\bar{\phi}}\right)$.[25] Both the Affine and Phantom models predict that the modulus is independent of N, which also differs from DN predictions, cf. Fig. (5(a)).

DN simulation results and predictions of the Affine and Phantom models in 2D are compared in Fig. 7. At fixed network topology, the Affine model agrees with DN predictions only near the density value ν^* for which $\bar{r}_0 = \sqrt{N}b$ in the DN model (for $\bar{\phi} = 4$, $\nu^* b^2 \approx 0.02$), whereas the Phantom model prediction meets the

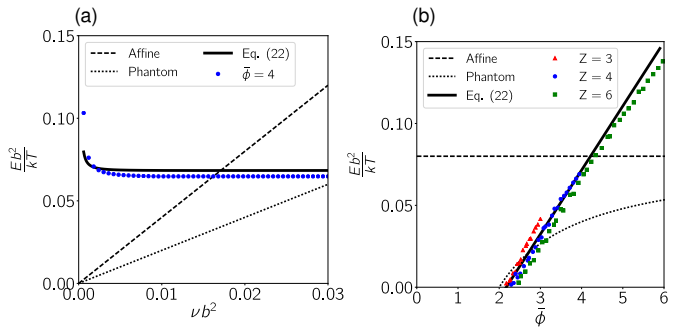

Fig. 7 (a) Evolution of the elastic modulus with density at constant coordination ($\bar{\phi} = 4$) with $N = 100$. (b) Evolution of modulus with average coordination at constant density ($\nu = \nu^*$) with $N = 100$ and $\nu b^2 = 0.02$.

DN curve only for a density value twice larger (Fig. 7(a)). At fixed density ($\nu = \nu^*$) (Fig. 7(b)), the Affine model meets the DN results near $\bar{\phi} = 4$. The Phantom model crosses the DN predictions at lower average coordination value, but predicts a different scaling of modulus with average coordination. In contrast, the simple estimate (22) together with relation (24) (continuous lines) well predicts the evolution of modulus with both density and coordination.

It is possible to extrapolate to 3D some of these scaling relations based on simple geometric considerations. Regarding the scaling of the initial chain end-to-end distance with density, a reasoning similar to the 2D case suggests that: $r_0 \sim \nu^{-1/3}$, independently of N. (Identifying the scaling of r_0 with average coordination would however require a computational investigation in 3D.) A simple estimate of the (shear) modulus using the Affine model in 3D then gives:

$$G = kT\nu\left(\frac{r_0^2}{Nb^2}\right) \sim \frac{\nu^{1/3}}{N}, \tag{25}$$

where the scaling holds at constant topology. This result again contradicts the classical result that G should be proportional to the density of chains and independent of the number of Kuhn segments, and is a direct consequence of the dependence of chain pre-straining on density.

The assumption that the initial end-to-end distance distribution is independent of density is reasonable for polymer networks which result from a random crosslinking process, such as vulcanisation or free-radical crosslinking copolymerisation. This is indeed the context in which rubber elasticity theory was developed in the first place. In vulcanisation processes, pre-existing linear chains are crosslinked randomly, leading to a broad molecular weight distribution.[6] Free-radical copolymerisation also lead to an irregular and spatially inhomogeneous network due to uncontrolled chain-growth and crosslinking.[5,55] The number of Kuhn segments in rubber elasticity theories must then be understood as an average value for a representative chains. In recent years advanced models have been proposed to account for molecular weight distribution in rubber-like materials.[56–58] This assumption becomes however questionable for networks produced by the coupling reaction of branched macromonomers with well-defined arm lengths, such as ideal tetra-arm PEG hydrogels. In such gels

it is expected that density of elastically effective chains, topology, and initial end-to-end distance distribution are all intrinsically coupled through the cross-coupling process in solution. For such networks, our results suggest that scaling relations between mechanical and network properties are different from those predicted by classical rubber elasticity theory.

Comparison to experimental data for near-ideal gels is needed to assess the validity of the proposed scaling relation (25). Notably, Sakai and coworkers investigated the effect of pre-polymer volume fraction and molecular weight on the elastic modulus of tetra-arm PEG hydrogels.[14,17] The density of elastically-effective chains was calculated from volume fraction and reaction efficiency using a tree-like approximation. These authors reported a shift in modulus from the Phantom prediction to the Affine prediction at around the overlapping polymer volume fraction with a super-linear rate. Interestingly, this trend can be explained neither by classical rubber elasticity theory, nor by our proposed 3D scaling. On the other hand, the elastic modulus was found to decrease with the number of Kuhn segments, in qualitative agreement with Eq. (25).[14] However, it is difficult to draw definitive conclusions on the relative contribution of density based on these experimental studies, because 1) there is an uncertainty on the actual value of the density of elastically-effective chains in the network, and 2) the topology of the network most likely changes as the volume fraction of pre-polymers increases. For example, a recent study based on kinetic graph theory and Monte Carlo simulation showed that the fraction of secondary loops decreases when the volume fraction increases.[59] Second-order loops are believed to have a significant impact on the elastic properties of polymer networks.[4,59] A couple of recent publications further pointed out that loop formation during gelation can lead to chain pre-straining, and that this factor should be accounted for in rubber elasticity theories.[60,61] The present study provides another indication that chain pre-straining associated with topological features can significantly impact the elastic behaviour, even in the absence of loops.

Regarding the maximum extensibility of the network, DN results in 2D indicate that $\lambda_{max} \sim \nu^{1/2} N$ at fixed topology, and that λ_{max} scales with $\bar{\phi}^{-1/2}$. In 3D, a measure based on the shortest path would predict that $\lambda_{max} \sim \nu^{1/3} N$ at fixed topology. (Identifying the role of topology on maximum extensibility in 3D requires a computational study.) This is different from classical theory, which predicts $\lambda_{max} \sim N^{1/2}$ in 2D and 3D, independent of density (and topology).

Experimental investigations for tetra-arm PEG gels suggested that $\lambda_{max} \sim v_p^{1/3} N^{2/3}$, where v_p is the volume fraction of pre-polymers.[15,62] Assuming that the density of elastically-effective chains is proportional to volume fraction, experimental findings thus confirm the DN predictions regarding the effect of density on the extensibility limit. On the other hand, the scaling exponent for N deduced from experiments appears to be intermediate between classical theory and DN prediction. As previously mentioned, the relative contribution of each network parameter is difficult to assess in experiments since the network topology is likely to change when the volume fraction and/or molecular weight of the pre-polymers is changed.

The generalisation of the DN modelling approach to 3D and confirmation of the anticipated scaling relations will be presented in a forthcoming study, together with direct comparison to experimental data. The effect of secondary loops on the elastic properties will also be investigated, alongside the effect of average coordination, density and number of Kuhn segments. Systematic comparison between DN predictions and non-Gaussian rubber elasticity theories in 3D will be carried out to assess their underlying assumptions, in particular regarding the partitioning of stretches among chains with different orientations.

6 Conclusion

We have developed of computational framework based on discrete networks to investigate the effect of network parameters on the mechanical properties of flexible polymer networks in two dimensions. In particular, the relative contributions of the density of elastically effective chains and average network coordination were investigated. Our results show different scaling relations between mechanical properties and network parameters than those predicted by classical rubber elasticity theories. Most notably, two-dimensional discrete network simulations show that the elastic modulus is independent of density at constant topology, and scales linearly with the average coordination. The discrepancy with rubber elasticity theory comes from different fundamental assumptions regarding the end-to-end distance distribution of the chains in the undeformed configuration of the network: while rubber elasticity theories assume that the distribution is independent of density and topology, in discrete network models the distribution is intrinsically coupled to the network parameters via the mechanical equilibrium equations. We hypothesise that the latter assumption is relevant for the study of the mechanical behaviour of networks formed by the coupling reaction of macromolecules in solution, such as ideal tetra-arm PEG hydrogels. Extension of the computational framework to three dimensions and comparison to experimental data are needed to validate this hypothesis.

Conflicts of interest

There are no conflicts of interest to declare.

Acknowledgements

G.A. is supported by a Monash Graduate Scholarship. The authors acknowledge fruitful discussions with Prof. J. Forsythe and Prof. R.P. Jagadeeshan from Monash University.

A 2D Affine model

The Affine model considers an assembly of long polymer chains that are randomly crosslinked at a relatively small number of points. It is assumed that the rms average end-to-end distance of the polymer strands between crosslink points is the same as that of a free chain, $r_0 = \lambda_0 \sqrt{N} b$. Since different polymer strands typically have different molecular weights, N actually represents the number of Kuhn segments of a representative chain. The stretch λ_0 represents the swelling stretch relative to the dry state. The chain density in the swollen and dry state are thus related by $\nu^{\mathrm{dry}} = \nu \lambda_0^2$. End-to-end vectors between crosslink points are

assumed to deform affinely with the macroscopic stretches λ_1 and λ_2 (with $\lambda_1\lambda_2 = 1$), measured relative to the swollen state. The components of a given end-to-end vector having components (x_0, y_0) in the pre-swollen state are thus:

$$x = \lambda_1 x_0, \quad y = \lambda_2 y_0. \tag{26}$$

The free energy of each chain in the network is given by Eq. (3). Summing the energies of the n (elastically-effective) chains in the network and dividing by the area A of the swollen network, the free energy density is obtained:

$$W = \frac{kT}{Nb^2}\frac{1}{A}\left[\lambda_1^2\left(\sum_{i=1}^{n} x_0^2\right) + \lambda_2^2\left(\sum_{i=1}^{n} y_0^2\right)\right] + C, \tag{27}$$

where C is a constant. Given that the chains are randomly distributed in the network, and using the above expression for the rms average r_0, we have:

$$\left(\sum_{i=1}^{n} x_0^2\right) = \left(\sum_{i=1}^{n} y_0^2\right) = \frac{n}{2} r_0^2 = \frac{n}{2}\lambda_0^2 N b^2. \tag{28}$$

Inserting the above result into Eq. (27), we finally obtain:

$$W = \frac{kT\nu}{2}\lambda_0^2(\lambda_1^2 + \lambda_2^2 - 2), \tag{29}$$

where we used $\nu = n/A$ and have identified the constant C by requiring the free energy to be zero in the unstrained state $\lambda_1 = \lambda_2 = 1$. Using Eq. (10), the stress-stretch relation is given by:

$$\sigma_1 - \sigma_2 = kT\nu\lambda_0^2\left(\lambda_1^2 - \frac{1}{\lambda_1^2}\right). \tag{30}$$

The corresponding modulus of the network, defined in Eq. (6), is:

$$E^{\text{aff}} = 4kT\nu\lambda_0^2 = 4kT\nu^{\text{dry}} \tag{31}$$

The latter equation indicates that, for a given dry network, the elastic modulus is independent of the degree of swelling. This can be understood as follows. Upon swelling of a network with fixed density ν^{dry}, chains are pre-strained and the energy of the network scales with λ_0^2, while concurrently the density decreases as $1/\lambda_0^2$. The increase in free energy associated with the decrease in entropy of the chains upon swelling exactly balances the effect of a lower density. This is different from the 3D case. In the 3D Affine model, the energy still scales with λ_0^2 due to chain straining during swelling, however the density decreases as $1/\lambda_0^3$, giving the classical relationship between the (shear) moduli in the swollen and dry states: $G = G^{\text{dry}}/\lambda_0$.[21]

Notes and references

1 J. Mark and B. Erman, *Rubberlike elasticity - A molecular primer, 2nd Ed.*, Cambridge University Press, 2007.

2 M. Shibayama, *Macromol. Chem. Phys.*, 1998, **199**, 1–30.

3 T. Sakai, Y. Akagi, T. Matsunaga, M. Kurakazu, U.-I. Chung and M. Shibayama, *Macromol. Rapid Commun.*, 2010, **31**, 1954–1959.

4 M. Zhong, R. Wang, K. Kawamoto, B. Olsen and J. Johnson, *Science*, 2016, **353**, 1264–1268.

5 S. Seiffert, *Polym. Chem.*, 2017, **8**, 4472–4487.

6 G. Hild, *Prog. Polym. Sci.*, 1998, **23**, 1019–1149.

7 Y. Okumura and K. Ito, *Adv. Mater.*, 2001, **13**, 485–487.

8 M. Lutolf and J. Hubbell, *Biomacromolecules*, 2003, **4**, 713–722.

9 M. A. Haque, T. Kurokawa and J. P. Gong, *Polymer*, 2012, **53**, 1805–1822.

10 Y. Gu, E. A. Alt, H. Wang, X. Li, A. P. Willard and J. A. Johnson, *Nature*, 2018, **560**, 65.

11 T. Sakai, T. Matsunaga, Y. Yamamoto, C. Ito, R. Yoshida, S. Suzuki, N. Sasaki, M. Shibayama and U.-I. Chung, *Macromolecules*, 2008, **41**, 5379–5384.

12 T. Matsunaga, T. Sakai, Y. Akagi, U.-I. Chung and M. Shibayama, *Macromolecules*, 2009, **42**, 1344–1351.

13 T. Matsunaga, T. Sakai, Y. Akagi, U.-I. Chung and M. Shibayama, *Macromolecules*, 2009, **42**, 6245–6252.

14 Y. Akagi, J. Gong, U.-i. Chung and T. Sakai, *Macromolecules*, 2013, **46**, 1035–1040.

15 Y. Akagi, T. Katashima, H. Sakurai, U.-i. Chung and T. Sakai, *RSC Adv.*, 2013, **3**, 13251–13258.

16 A. Zhang, J. Ling, K. Li, G. Fu, T. Nakajima, T. Nonoyama, T. Kurokawa and J.-P. Gong, *J. Polym. Sci.*, 2016, **54**, 1227–1236.

17 K. Nishi, K. Fujii, U.-i. Chung, M. Shibayama and T. Sakai, *Phys. Rev. Lett.*, 2017, **119**, 267801.

18 H. Kamata, Y. Akagi, Y. Kayasuga-Kariya, U.-i. Chung and T. Sakai, *Science*, 2014, **343**, 873–875.

19 K.-i. Hoshino, T. Nakajima, T. Matsuda, T. Sakai and J. Gong, *Soft Matter*, 2018, **14**, 9693–9701.

20 G. Parada and X. Zhao, *Soft Matter*, 2018, **14**, 5186–5196.

21 L. Treloar, *The physics of rubber elasticity*, Oxford University Press, 1975.

22 F. Wall, *J. Chem. Phys.*, 1942, **10**, 132–134.

23 P. J. Flory, *Principles Of Polymer Chemistry*, Cornell University Press, Ithaca, 1953.

24 H. James, *J. Chem. Phys.*, 1947, **15**, 651–668.

25 P. Flory, *Proc. R. Soc. Lond. A*, 1976, **351**, 351–380.

26 M. Wang and E. Guth, *J. Chem. Phys.*, 1952, **20**, 1144–1157.

27 L. Treloar, *Trans. Faraday Soc.*, 1946, **42**, 83–94.

28 E. Arruda and M. Boyce, *J. Mech. Phys. Solids*, 1993, **41**, 389–412.

29 P. Wu and E. Van Der Giessen, *J. Mech. Phys. Solids*, 1993, **41**, 427–456.

30 M. C. Boyce and E. M. Arruda, *Rubber Chem. Technol.*, 2000, **73**, 504–523.

31 P. De Gennes, *J. Phys. Lett.*, 1976, **37**, 1–2.

32 S. Feng and P. Sen, *Phys. Rev. Lett.*, 1984, 216–219.

33 Y. Kantor and I. Webman, *Physical Review Letters*, 1984, **52**, 1891–1894.

34 W. Tang and M. Thorpe, *Phys. Rev. B*, 1988, 5539–5551.

35 S. Arbabi and M. Sahimi, *Phys. Rev. B*, 1993, **47**, 695–702.

36 H. Qi, C. Ortiz and M. Boyce, *J. Eng. Mater. Technol.*, 2006,

128, 509–518.
37 I. Salib, G. Kolmakov, B. Bucior, O. Peleg, M. Kröger, T. Savin, V. Vogel, K. Matyjaszewski and A. Balazs, *Langmuir*, 2011, **27**, 13796–13805.
38 A. Sugimura, M. Asai, T. Matsunaga, Y. Akagi, T. Sakai, H. Noguchi and M. Shibayama, *Polym. J.*, 2013, **45**, 300–306.
39 K. Kothari, Y. Hu, S. Gupta and A. Elbanna, *J. Appl. Mech.*, 2018, **85**, 031008.
40 R. Picu, *Soft Matter*, 2011, **7**, 6768–6785.
41 C. Broedersz and F. MacKintosh, *Rev. Mod. Phys.*, 2014, **86**, 995–1036.
42 D. Boal, *Mechanics of the cell, 2nd edition*, Cambridge University Press, 2012.
43 J. Hansen, R. Skalak, S. Chien and A. Hoger, *Biophys. J.*, 1996, **70**, 146–166.
44 D. Discher, D. Boal and S. Boey, *Biophys. J.*, 1998, **75**, 1584–1597.
45 J. Li, M. Dao, C. Lim and S. Suresh, *Biophys. J.*, 2005, **88**, 3707–3719.
46 D. Hartmann, *Biomech. Model. Mechanobiol.*, 2010, **9**, 1–17.
47 M. Chen and F. Boyle, *Mater. Sci. Eng. C*, 2014, **43**, 506–516.
48 K. Nishi, H. Noguchi, T. Sakai and M. Shibayama, *J. Chem. Phys.*, 2015, **143**, 184905.
49 C. Geuzaine and J.-F. Remacle, *Int. J. Numer. Meth. Eng.*, 2009, **79**, 1309–1331.
50 M. Rubinstein and R. Colby, *Polymer Physics*, Oxford University Press, 2003.
51 S. Iliafar, D. Vezenov and A. Jagota, *Eur. Polym. J.*, 2014, **51**, 151–158.
52 S. Plimpton, *J. Comput. Phys.*, 1995, **117**, 1–19.
53 M. Abramowitz and I. A. Stegun, *Handbook of mathematical functions: with formulas, graphs, and mathematical tables*, Courier Corporation, 1965, vol. 55.
54 E. Dijkstra, *Numer. Math.*, 1949, **1**, 269–271.
55 A. Matsumoto, in *Synthesis and Photosynthesis*, Springer, 1995, vol. 123 of Adv. Polym. Sci., pp. 41,80.
56 M. Itskov and A. Knyazeva, *Int. J. Solids Struct.*, 2016, **80**, 512 – 519.
57 E. Verron and A. Gros, *J. Mech. Phys. Solids*, 2017, **106**, 176–190.
58 M. Tehrani and A. Sarvestani, *Eur. Polym. J.*, 2017, **87**, 136–146.
59 T.-S. Lin, R. Wang, J. Johnson and B. Olsen, *Macromolecules*, 2018, **51**, 1224–1231.
60 M. Lang, *ACS Macro Lett.*, 2018, **7**, 536–539.
61 T.-S. Lin, R. Wang, J. Johnson and B. Olsen, *Macromolecules*, 2019, **52**, 1685–1694.
62 S. Kondo, U.-i. Chung and T. Sakai, *Polymer J.*, 2014, **46**, 14–20.